






Article

Comparison of Proton Acceptor and Proton Donor Properties of H₂O and H₂O₂ in Organic Crystals of Drug-like Compounds: Peroxosolvates vs. Crystallohydrates

Mikhail V. Vener ^{1,*}, Andrei V. Churakov ¹, Alexander P. Voronin ², Olga D. Parashchuk ³,
Sergei V. Artobolevskii ⁴, Oleg A. Alatorsev ⁴, Denis E. Makhrov ⁴, Alexander G. Medvedev ¹
and Aleksander Filarowski ^{5,*}

¹ Kurnakov Institute of General and Inorganic Chemistry, Russian Academy of Sciences, Leninskii Prosp. 31, 119991 Moscow, Russia; churakov@igic.ras.ru (A.V.C.); mag@igic.ras.ru (A.G.M.)

² G.A. Krestov Institute of Solution Chemistry RAS, 153045 Ivanovo, Russia; apv@isc-ras.ru

³ Faculty of Physics, Lomonosov Moscow State University, 119991 Moscow, Russia; olga_par@physics.msu.ru

⁴ Faculty of Natural Science, Mendeleev University of Chemical Technology, Miusskaya Square 9, 125047 Moscow, Russia; Artobolevskiy_Sergey_Vladimirovich@muctr.ru (S.V.A.); Olegalatorcev@muctr.ru (O.A.A.); Denis_Makhrov@muctr.ru (D.E.M.)

⁵ Faculty of Chemistry, University of Wrocław 14 F. Joliot-Curie Str., 50-383 Wrocław, Poland

* Correspondence: vener@igic.ras.ru (M.V.V.); aleksander.filarowski@chem.uni.wroc.pl (A.F.)



Citation: Vener, M.V.; Churakov, A.V.; Voronin, A.P.; Parashchuk, O.D.; Artobolevskii, S.V.; Alatorsev, O.A.; Makhrov, D.E.; Medvedev, A.G.; Filarowski, A. Comparison of Proton Acceptor and Proton Donor Properties of H₂O and H₂O₂ in Organic Crystals of Drug-like Compounds: Peroxosolvates vs. Crystallohydrates. *Molecules* **2022**, *27*, 717. <https://doi.org/10.3390/molecules27030717>

Academic Editor: Aleksandar Milosavljević

Received: 2 December 2021

Accepted: 19 January 2022

Published: 22 January 2022

Publisher's Note: MDPI stays neutral with regard to jurisdictional claims in published maps and institutional affiliations.



Copyright: © 2022 by the authors. Licensee MDPI, Basel, Switzerland. This article is an open access article distributed under the terms and conditions of the Creative Commons Attribution (CC BY) license (<https://creativecommons.org/licenses/by/4.0/>).

Abstract: Two new peroxosolvates of drug-like compounds were synthesized and studied by a combination of X-ray crystallographic, Raman spectroscopic methods, and periodic DFT computations. The enthalpies of H-bonds formed by hydrogen peroxide (H₂O₂) as a donor and an acceptor of protons were compared with the enthalpies of analogous H-bonds formed by water (H₂O) in isomorphous (isostructural) hydrates. The enthalpies of H-bonds formed by H₂O₂ as a proton donor turned out to be higher than the values of the corresponding H-bonds formed by H₂O. In the case of H₂O₂ as a proton acceptor in H-bonds, the ratio appeared reversed. The neutral O⋯H-O/O⋯H-N bonds formed by the lone electron pair of the oxygen atom of water were the strongest H-bonds in the considered crystals. In the paper, it was found out that the low-frequency Raman spectra of isomorphous crystalline hydrate and peroxosolvate of N-(5-Nitro-2-furfurylidene)-1-aminohydantoin are similar. As for the isostructural hydrate and peroxosolvate of the salt of protonated 2-amino-nicotinic acid and maleic acid monoanion, the Raman spectra are different.

Keywords: crystal packing; periodic DFT computations; bifurcate hydrogen bonds; low-frequency Raman spectroscopy; hydrogen bond enthalpy

1. Introduction

In the last decade, the development of drug-like cocrystals became one of the topical issues in pharmaceutical chemistry [1–3], owing to a possible synergetic effect of their components [4]. The hydrogen peroxide crystalline complexes look very promising since H₂O₂ demonstrates a wide spectrum of antimicrobial activity [5]. Recently, the peroxosolvate of the antifungal drug “miconazole” was synthesized and structurally characterized [6]. However, upon storage, peroxosolvates get decomposed with hydrogen peroxide leaking away, and, therefore, they are not applicable for medical treatment. The formation of stoichiometric H₂O₂ adduct with no loss of oxidizing ability upon long-term storage is one of key challenges [7]. It is well-known that the stability of peroxosolvates is governed by the strength and amount of hydrogen bonds formed by peroxide molecules [8,9] and the topology of H-bonded networks within their crystals [10,11].

The conventional hydrogen bonds (H-bonds) are the main type of intermolecular interaction in crystallohydrates and crystalline peroxosolvates. Water and hydrogen peroxide are able to form a different number of H-bonds in multicomponent organic crystals. H₂O

usually forms three H-bonds: either two bonds as a proton donor and one bond as a proton acceptor or vice versa [11–13]. H₂O₂ always forms two conventional H-bonds as a proton donor and may form up to four H-bonds as a proton acceptor [14]. The proton-donor atoms are usually formed with aromatic nitrogen, N_{AR} [9], and the [−]O-N⁺_{AR} [10], [−]O₂CR [15], O=CR₂ [16] groups. Such H-bonds are quasi-linear (the O-H⋯O/O-H⋯N angle is greater than 160 degrees) and are of moderate strength [9,15,16]. H₂O₂ forms three or four H-bonds as a proton acceptor in a few crystals [9]. These bonds are formed between lone electron pairs of the oxygen atom of H₂O₂ and π-conjugated amino groups of organic cofomers [9]. They are characterized by an almost linear O⋯H-N fragment and are relatively weak [9,16]. The H₂O₂ molecule forms one or two H-bonds as a proton acceptor in about half of the peroxosolvates [14]. A significant number of these crystals contain zwitterions [17–19]. The oxygen of the H₂O₂ molecule and the ⁺H₃N- group of the amino acid zwitterion often form nonlinear H-bonds (the O⋯H-N⁺ angle is less than 140 degrees), Figure S1.

The distance between the A and B atoms (*R*(A⋯B)) of the A-H⋯B fragment, where A and B are O, N, F and others, plays a crucial role in geometry, dynamics, and in the energy of the H-bond network [20,21]. The different properties of H-bonds are determined by the *R*(A⋯B) distance, in particular, the energy/enthalpy of H-bond (*E*_{HB}/*ΔH*_{HB}). The proposed empirical schemes made it possible to estimate the *E*_{HB} values from *R*(O⋯O) [22,23]. These approaches are limited to the O-H⋯O fragment in the solid state. More universal approaches use the frequency shifts of the O-H stretching vibrations [24], the H⋯O distance [25,26] and the electron density at the bond critical point [27]. The pros and cons of various schemes for *E*_{HB}/*ΔH*_{HB} estimating are given elsewhere [28]. In the present study, the *ΔH*_{HB} values were evaluated using the Rozenberg equation [25]:

$$-\Delta H_{HB} [\text{kJ mol}^{-1}] = 0.134 \cdot R(\text{H}\cdots\text{O})^{-3.05}, \quad (1)$$

where the *R*(H⋯O) is the H⋯O distance (nm). The empirical correlation (1) gives the *ΔH*_{HB} values of intermolecular H-bonds in molecular crystals in the range of 10–80 kJ/mol with the accuracy around several kJ/mol [25]. The Equation (1) is a powerful “toolbox” for studying crystals consisting of H-bonds of different strengths and types, including ionic or charged fragments [25,26]. The main limitation of equation (1) is the accuracy of experimental measurements of the position of hydrogen in H-bridge. Therefore, the use of the neutron diffraction method is necessary. Nevertheless, the number of crystals with H-bonds studied by this method is very limited [29]. In the present study, the exact values of the H⋯O distances were computed using the periodic DFT methods [30,31].

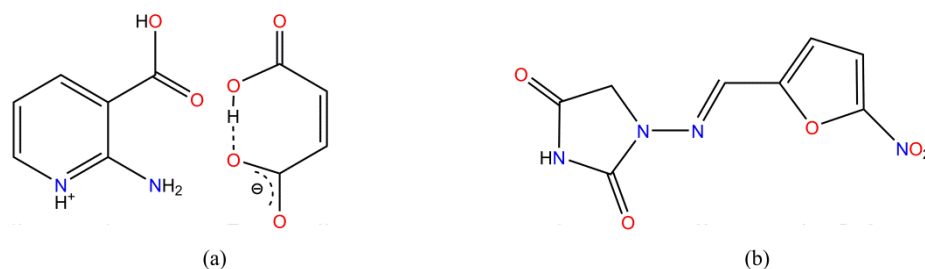
The energy/enthalpy of H-bonds in peroxosolvates composed by H₂O₂ as a proton donor is usually greater than the corresponding *E*_{HB}/*ΔH*_{HB} of H-bonds formed by the H₂O molecule [15,32]. A systematic comparison of the *E*_{HB}/*ΔH*_{HB} values of H-bonds formed by H₂O and H₂O₂ as proton acceptors has not been performed so far. In paper [13] it is believed that the energies of moderately strong H-bonds of complexes formed by the H₂O molecule as a proton donor or a proton acceptor are approximately equal. As for multicomponent organic crystals, this equality may not be observed, since the energies of the H-bonds formed by H₂O and H₂O₂ as proton acceptors are determined by the nature of the organic molecule. Indeed, the *E*_{HB}/*ΔH*_{HB} values of the H-bond built up by the H₂O molecule as a proton acceptor with a diglycine cyclic dipeptide are greater than the values of the corresponding H-bond formed by H₂O₂ [32]. Obviously, an accurate comparison of the energy of the H-bond formed by H₂O and H₂O₂ as acceptors of protons in the solid state involves the study of multicomponent organic crystals that form isomorphous (isostructural) hydrates and peroxosolvates.

To compare the proton acceptor and proton donor properties of H₂O and H₂O₂ in multicomponent organic crystals, the following issues were consistently resolved in this work.

1. The features of H-bonded networks in hydrates and isomorphous peroxosolvates of multicomponent organic crystals were identified using the Cambridge Structural

Database version 5.42 (September 2021) [33] and version 2016-1 of the Inorganic Crystal Structure Database [34].

- The H-bond enthalpy in crystalline hydrates ([2-amino-nicotinic acid+maleic acid+H₂O] (1:1:1), [N-(5-Nitro-2-furfurylidene)-1-aminohydantoin+H₂O] (1:1)) and peroxosolvates ([2-amino-nicotinic acid+maleic acid+H₂O₂] (1:1:1), [N-(5-Nitro-2-furfurylidene)-1-aminohydantoin+H₂O₂] (1:1)) (Scheme 1) was determined using periodic DFT calculations [30] followed by Rosenberg's equation [23,24]. The structures of the crystalline hydrates were studied by X-ray diffraction [35,36]. The isomorphous or isostructural peroxosolvates were purposefully prepared for this study.



Scheme 1. Structures of salts of protonated 2-amino-nicotinic acid and maleic acid monoanion (a) and N-(5-Nitro-2-furfurylidene)-1-aminohydantoin (b).

- The spectroscopic features of the considered crystals were studied by low-frequency Raman spectroscopy followed by periodic DFT computations.

2. Results and Discussion

2.1. Features of H-Bonded Networks in Hydrates and Isomorphous Peroxosolvates

Our statistics are based on 103 peroxosolvates, 91 of which are organic crystals' structures [33,34]. The detailed analysis of these crystals' structures is given in Tables S1 and S2 of Ref. [28]. After excluding structures with structurally disordered H₂O₂ molecules and structures with non-alkaline metals, the number of peroxosolvates decreased to 56. Furthermore, those structures were excluded in which H₂O₂ molecules interact directly with the Li⁺, Na⁺, K⁺, NH₄⁺ ions or with other H₂O₂ molecules through H-bonds. The crystals containing the other solvent molecules were also excluded from consideration. As a result, the final number of analyzed peroxosolvates was 46. We concluded the following: (1) H₂O₂ does not form H-bonds as a proton acceptor if the organic cofomers do not have active hydrogen atoms. Such crystals make up a significant proportion of the considered structures (20). (2) H₂O₂ forms three or four H-bonds as a proton acceptor in five structures. The oxygen atoms of H₂O₂ are less likely to participate in bifurcate H-bonds than the C=O and P=O groups [20,37]. (3) In the remaining structures (21), the H₂O₂ molecule forms one or two bonds as a proton acceptor. If the cofomer is not a zwitterion, then H₂O₂ can form the quasi-linear O⋯H-N bonds (Figure S2). (4) Currently, there is only one example of the bifurcate H-bond formed by the OH group of H₂O₂ [38]. Refcodes of the analyzed peroxosolvates are given in Table S2. Analysis of secondary interactions, in particular, O⋯H-C bonds [39,40], is beyond the scope of this work.

The comparison of the metric and energy characteristics of H-bonds formed by the H₂O₂ and H₂O molecules in the solid state involves the use of isomorphous peroxosolvates and crystalline hydrates. Notably, the number of such structures is not large. By means of a special choice of cofomers (cyclic N-oxides), isomorphous crystal hydrates and peroxosolvates containing only two H-bonds formed by H₂O and H₂O₂ as a proton donor were studied in ref. [10]. It was stated that H₂O₂ forms shorter H-bonds as compared to H₂O. A similar trend was previously revealed in refs. [15,32] in isomorphous crystalline hydrates and peroxosolvates of several amino acids. These studies show that the hydrogen peroxide molecule usually forms shorter (strong) donor H-bonds than the water molecule. Data on the proton acceptor properties of H₂O₂ and H₂O in the solid state are scarce. The values of the O⋯H-N⁺ bond energy are comparable in isomorphous crystalhydrate and

peroxosolvate of serine [15]. The $O\cdots H-N$ bond energy in the crystalline hydrate of the cyclic dipeptide is much higher than that in the isomorphous peroxosolvate [32]. This issue required an additional study, which was performed in the next section.

2.2. The H-Bond Enthalpy in the Selected Crystalline Hydrates and Peroxosolvates

Crystalline [2-amino-nicotinic acid+maleic acid+ H_2O] (1:1:1), denoted below as [2AmNic+Mle+ H_2O], is a relevant object for the following reasons. Firstly, H_2O forms three quasi-linear H-bonds in this crystal—two as a proton donor and one as a proton acceptor [36]. Secondly, the structure, the spectrum, and the E_{HB}/H values of H-bond in this crystal were characterized by X-ray analysis, terahertz Raman spectroscopy, and periodic DFT calculations [36]. In this work, we accomplished the synthesis of peroxosolvate [2AmNic+Mle+ H_2O_2] (1:1:1) (Section 3.3). The network of H-bonds formed by H_2O_2 in this crystal is equivalent to the network of H-bonds formed by H_2O in crystalline (cf. [2AmNic+Mle+ H_2O_2] and [2AmNic+Mle+ H_2O], Figure 1). These crystals are isostructural. Crystalline [*N*-(5-Nitro-2-furfurylidene)-1-aminohydantoin+ H_2O] (1:1) [35], denoted below as [NFA+ H_2O] (Figure 2), was chosen as the second model of crystalline hydrate. In this crystal, the H_2O molecule forms one quasi-linear H-bond as a proton acceptor and three H-bonds as a proton donor, with one of the OH groups forming a bifurcate bond. Unlike [2AmNic+Mle+ H_2O] crystal, in the [NFA+ H_2O] crystal a water molecule forms H-bonds as a proton donor with the same neutral molecule, whereas H-bond as a proton acceptor is formed with the H-N group of a neighboring molecule. Moreover, we obtained peroxosolvate [NFA+ H_2O_2] (1:1), isomorphous to this crystalline hydrate (Figure 2). The network of H-bonds in the synthesized [NFA+ H_2O_2] is presented in Figure 2b.

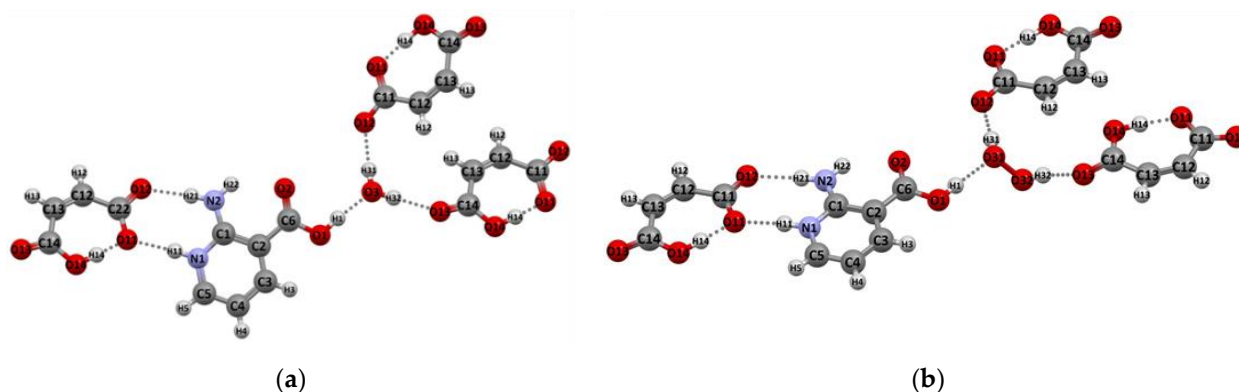


Figure 1. The fragments of the [2AmNic+Mle+ H_2O] [36] (a) and [2AmNic+Mle+ H_2O_2] (b) structures. H-bonds are denoted by dotted lines.

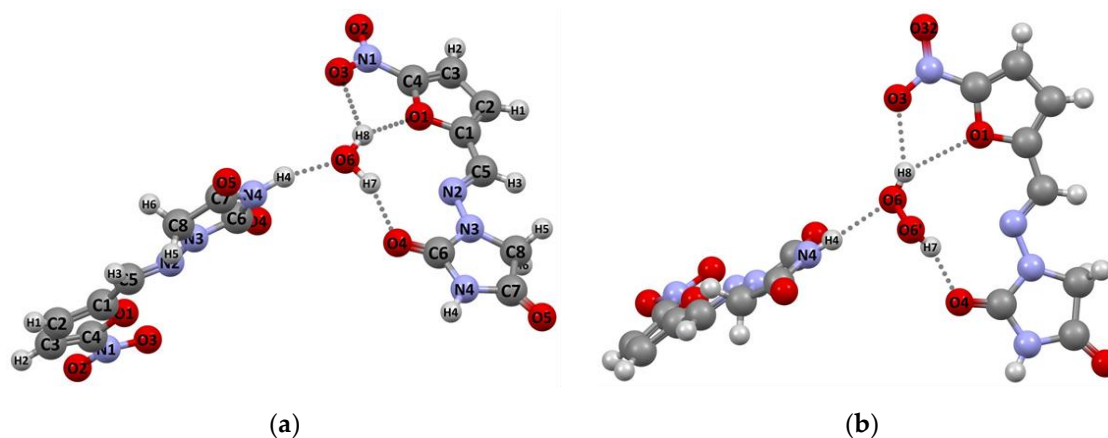


Figure 2. The fragments of the [NFA+ H_2O] [35] (a) and [NFA+ H_2O_2] (b) structures. H-bonds are denoted by dotted lines.

The theoretical values of the enthalpy of intermolecular H-bonds in the considered crystals were evaluated using the equation (1), where the O...H distances were calculated at the PBE-D3/6-31G** level (Table 1). In accordance with the literature data [30,31] the relaxed values of the O...H distance in molecular crystals systematically exceed the X-ray values by ~0.15 Å. The deviations from this parameter are due to serious differences between the theoretical distances A...B and the experimental ones.

Table 1. Distances between the atoms involved in the formation of intermolecular H-bonds in [2AmNic+Mle+H₂O], [2AmNic+Mle+H₂O₂], [NFA+H₂O] and [NFA+H₂O₂]; $R(\text{O}\cdots\text{N})$, $R(\text{O}\cdots\text{O})$, and $R(\text{H}\cdots\text{O})$ obtained using periodic DFT computations (PBE-D3/6-31G**) and the ΔH_{HB} values evaluated using Equation (1).

Fragment ¹	$R(\text{O}\cdots\text{N})/R(\text{O}\cdots\text{O})$, ² Å	$R(\text{H}\cdots\text{O})$, Å	ΔH_{HB} , kJ/mol
[2AmNic+Mle+H ₂ O] (1:1:1)			
O12 ... H21-N2	2.804 (2.816)	1.777 (1.928)	26.0
O11 ... H11-N1	2.816 (2.816)	1.770 (1.905)	26.4
O12 ... H31-O3	2.701 (2.717)	1.707 (1.860)	29.4
O13 ... H32-O3	2.765 (2.771)	1.783 (1.900)	25.8
O3 ... H1-O1	2.536 (2.567)	1.484 (1.641)	45.1
[2AmNic+Mle+H ₂ O ₂] (1:1:1)			
O12 ... H21-N2	2.846 (2.831)	1.810 (1.955)	24.6
O11 ... H11-N1	2.849 (2.735)	1.805 (1.803)	24.8
O12 ... H31-O31	2.658 (2.636)	1.648 (1.759)	32.8
O13 ... H32-O32	2.774 (2.698)	1.841 (1.767)	23.3
O31 ... H1-O1	2.726 (2.646)	1.738 (1.769)	27.9
[NFA+H ₂ O]			
N4-H4 ... O6	2.689 (2.763)	1.653 (1.782)	32.5
O6-H7 ... O4	2.834 (2.961)	1.938 (2.015)	20.0
O6-H8 ... O1	3.080 (3.148)	2.338 (2.245)	11.3
O6-H8 ... O3	2.966 (3.172)	2.100 (2.392)	15.6
[NFA+H ₂ O ₂]			
N4-H4 ... O6	2.807 (2.905)	1.822 (2.098)	24.1
O6'-H7 ... O4	2.735 (2.737)	1.786 (1.894)	25.6
O6-H8 ... O1	3.175 (3.128)	2.496 (2.477)	9.2
O6-H8 ... O3	2.871 (2.907)	1.935 (2.144)	20.1

¹ the atomic numbering is given in Figures 1 and 2; ² experimental values are given in parentheses.

To estimate the error in determining the ΔH_{HB} parameter caused by a significant deviation of the theoretical $R(\text{H}\cdots\text{O})$ values from the experimental ones, the $R(\text{H}\cdots\text{O})$ values were computed at the B3LYP/6-31G** level (Tables S2 and S3). The ΔH_{HB} values calculated at the B3LYP/6-31G** level agree nicely with those obtained using the PBE-D3/6-31G** level (cf. Table 1 with Tables S2 and S3). In accordance with the literature [41,42], the PBE-D3 calculations slightly overestimate the H-bonded energy compared to the B3LYP calculations.

The enthalpies of H-bonds formed by H₂O₂ as a proton donor turned out to be higher or comparable with the values of the corresponding H-bonds formed by H₂O [15,32,43]. In the case of H-bonds formed by H₂O₂ and H₂O as a proton acceptor, the picture is reversed. In accordance with the literature data [32], the enthalpy of H-bonds formed by H₂O as a proton acceptor is systematically higher than the analogous values of H-bonds formed by H₂O₂.

As it follows from the data (Table 1), the value of the enthalpy of the bifurcate H-bond formed by the OH group is significantly higher than the enthalpy of the ordinary H-bond formed by another OH group of H₂O or H₂O₂.

2.3. Low-Frequency Raman Spectra of the Considered Crystals

Low-frequency Raman spectroscopy is widely used in the investigation of organic materials [44]. A special attention is paid to intermolecular interactions [45–47], in particular, H-bonds [48]. We showed that B3LYP and PBE-D3 with fixed cell parameters provide

a reasonable description of the low-frequency Raman spectra of the multicomponent molecular crystals [26,49]. In this work, the Raman spectra of the considered crystals were investigated in the 10–2000 cm^{-1} frequency region for two purposes (Figure 3). Firstly, to identify possible differences in the low-frequency Raman spectra of crystallohydrates and isomorphous peroxolvates. Secondly, to find out how well the periodic DFT computations with the 6-31G** basis set reproduce the Raman spectra of the considered crystals in the mid-frequency range.

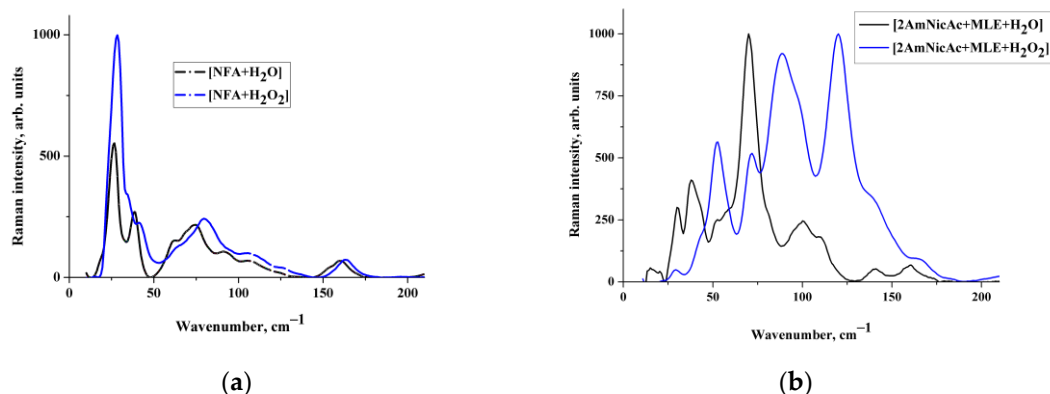


Figure 3. The experimental low-frequency Raman spectra of the [NFA+H₂O] and [NFA+H₂O₂] complexes (a); the [2AmNic+Mle+H₂O] and [2AmNic+Mle+H₂O₂] complexes (b).

Crystalline [NFA+H₂O] is isomorphous to crystalline [NFA+H₂O₂] (Table 2). Their experimental low-frequency spectra are very similar (Figure 3a). The situation is different for crystalline [2AmNic+Mle+H₂O] and crystalline [2AmNic+Mle+H₂O₂] (Figure 3b). This result can be explained by the fact that the latter crystals have a similar network of H-bonds, but their crystal structure is different (Table 2 and data from refs [35,36]).

Table 2. Crystal data and refinement details of the [2AmNic+Mle+H₂O₂] and [NFA+H₂O₂] structures.

	[2AmNic+Mle+H ₂ O ₂]	[NFA+H ₂ O ₂]
Empirical formula	C ₁₀ H ₁₂ N ₂ O ₈	C ₈ H ₈ N ₄ O ₇
<i>F</i> _w	288.22	272.18
color, habit	colorless, prism	light-yellow, prism
crystal size (mm)	0.25 × 0.20 × 0.15	0.25 × 0.15 × 0.10
crystal system	monoclinic	orthorhombic
space group	<i>P</i> 2 ₁ / <i>n</i>	<i>P</i> bca
<i>a</i> (Å)	9.5451(4)	13.0154(7)
<i>b</i> (Å)	11.7871(4)	9.4659(7)
<i>c</i> (Å)	11.0780(4)	17.9512(10)
β (deg)	105.089(1)	90
<i>V</i> (Å ³)	1203.40(8)	2211.6(2)
<i>Z</i>	4	8
<i>D</i> _c (g·cm ^{−3})	1.591	1.635
μ (mm ^{−1})	0.140	0.146
<i>F</i> (000)	600	1120
θ range (deg)	2.51 to 29.00	2.27 to 28.00
refl colld	11941	19769
indep reflns/ <i>R</i> _{int}	3189/0.0219	2671/0.0650
reflns <i>I</i> > 2 σ (<i>I</i>)	2742	1995
No of param	229	205
GooF on <i>F</i> ²	1.047	1.025
<i>R</i> ₁ (<i>I</i> > 2 σ (<i>I</i>))	0.0345	0.0371
<i>wR</i> ₂ (all data)	0.0954	0.0882
largest diff peak/hole (e·Å ^{−3})	0.368/−0.191	0.250/−0.244

The PBE-D3/6-31G** and B3LYP/6-31G** calculations describe the low-frequency Raman spectra of crystalline [NFA+H₂O₂] (Figure 4). The computed wavenumbers of the most bands are bathochromically shifted, which is a common occurrence for harmonic frequencies of molecular crystals calculated using all-electronic Gaussian-type orbital bases [50]. The most intense band (~30 cm⁻¹) is characterized by the essential displacements of the oxygen atoms of H₂O₂ and the librations (rotations) of the five-member rings of NFA. The atomic displacements of the H₂O₂ molecule are negligible in the band around 80 cm⁻¹ (c.f. Figure 4b,c). The low-frequency Raman spectra of crystalline [NFA+H₂O] are compared with the theoretical ones in Figure S3. Such as in the case of the isomorphous peroxosolvate, the intense band of the water molecule vibrations did not occur in the low region (Figure S4a,b). Therefore, low-frequency Raman spectroscopy seems to be hardly applicable to distinguish between the crystalline hydrates of NFA. Similar results were obtained for [2AmNic+Mle+H₂O₂] and [2AmNic+Mle+H₂O]. In these crystals, no intense Raman band was observed, which could be assigned to vibrations of H₂O₂ (Figure 5b,c) or H₂O (Figure S6a,b).

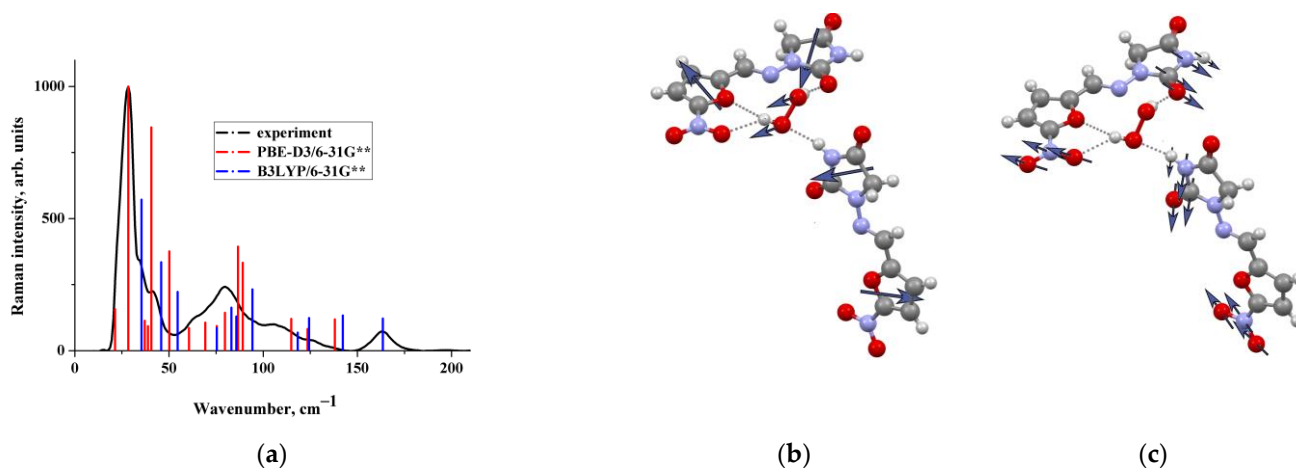


Figure 4. The experimental (black line) and calculated (PBE-D3—red sticks and B3LYP—blue sticks) low-frequency Raman spectra of the [NFA+H₂O₂] crystal (a). The height of the bars is proportional to the relative Raman intensity of corresponding transition. The schematic representation of the atom displacements of the two Raman intense vibrations (PBE-D3/6-31G**) at 30 cm⁻¹ (b) and 80 cm⁻¹ (c).

In the three crystals studied, the theoretical spectrum is in good agreement with the experimental one (Figure 4a, Figures S3 and S5). To harmonize the agreement between the experimental and theoretical Raman spectra of crystalline [2AmNic+Mle+H₂O₂] in the low-frequency region, a scaling factor of 0.9 was used (Figure 5a). Possible reasons for using a scaling factor for a single crystal are as follows. Scaling factors were developed for isolated molecules simpler than molecular crystals [51]. The low-frequency Raman-active vibrations in molecular crystals are mainly associated with the librational motions (Figure 1 in [52]). An additional reason for the difference between the calculated and experimental frequencies in the region below 200 cm⁻¹ may be crystal packing effects. In the case of the studied isomorphous crystals, this error is the same for [NFA+H₂O] and [NFA+H₂O₂]. Crystals of 2-amino-nicotinic acid have different symmetry groups (Table 2), and the error in the calculation of the wavenumbers of low-frequency vibrations differs for [2AmNic+Mle+H₂O] and [2AmNic+Mle+H₂O₂].

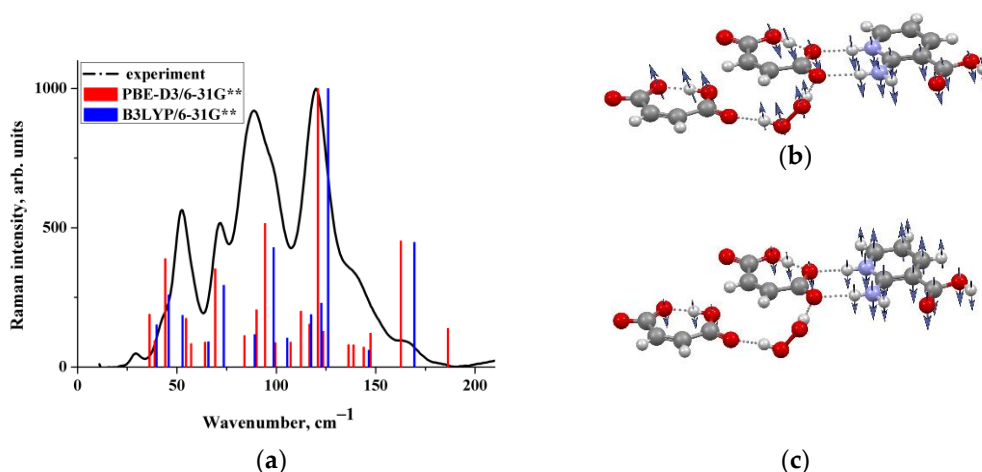


Figure 5. The experimental (black line) and calculated (PBE-D3—red sticks and B3LYP—blue sticks) low-frequency Raman spectra of the [2AmNic+Mle+H₂O₂] crystal (a). The theoretical values of wavenumbers are scaled by 0.9. The height of the bars is proportional to the relative Raman intensity of the corresponding transition. The schematic representation of the atom displacements of the two Raman intense vibrations (PBE-D3/6-31G**) at 44 cm⁻¹ (b) and 94 cm⁻¹ (c).

The O–O stretching vibration of H₂O₂ is located at 870 cm⁻¹ in crystalline peroxosolvates [53,54]. To check the stability of the considered peroxosolvates after laser excitation during Raman measurements, the obtained spectra were investigated in the frequency range of 850–950 cm⁻¹ and compared with the results of periodic DFT calculations (Figures S7 and S8). The experimental spectra of crystalline [NFA+H₂O₂] and crystalline [2AmNic+Mle+H₂O₂] do have Raman active bands around 880–890 cm⁻¹. The calculated vibration at 910 cm⁻¹ in both theoretical spectra corresponds to the O–O stretching vibration of H₂O₂.

3. Materials and Methods

3.1. Compounds and Solvents

Anhydrous NFA (CAS no. 67-20-9) with purity of 98% was purchased from Sigma-Aldrich (St. Louis, MO, USA) and used without additional purification. The 2-aminonicotinic acid (5345-47-1, 98%) was purchased from Sigma-Aldrich, and the maleic acid (110-16-7, 98%) was bought from Merck KGaA (Darmstadt, Germany).

The salt hydrate [2AmNic+Mle+H₂O] (1:1:1) was obtained according to the method described in the work by Surov et al. [36]. A stoichiometric mixture of 2AmNic and Mle was suspended in water to form a slurry and stirred on a magnetic stirrer overnight.

96% hydrogen peroxide. Danger of explosion! 100 mL of laboratory reagent grade 60% H₂O₂ (Fisher Scientific, Loughborough, UK) was concentrated to approximately 25 mL with an exhaustively cleaned rotary evaporator without the use of any vacuum grease (temperature exactly 50 °C and pressure 8 mbar). The concentration of the residual solution was examined by refractometry ($n_D = 1.403$ at 20°) [55].

3.2. Cocrystal Preparation

[2AmNic+Mle] and [NFA] were being dried in a treating oven for 5 h (80 °C, 100 mbar). 50 mg of unsolvated [2AmNic+Mle] or [NFA] were put into 2 mL vial and 1 mL of 96% hydrogen peroxide was added. The vials were tightly capped. The starting materials were dissolved by an intensive shaking of the vials at 50 °C. The obtained transparent solutions were stored in the freezer for one week at −23 °C. In both cases, high quality crystals (with dimensions up to 0.5 mm) were obtained. Afterwards, the surplus mother liquids were immediately removed from the cold vials using Pasteur pipets.

3.3. Single Crystal X-ray Diffraction

The diffraction intensities for [2AmNic+Mle+H₂O₂] and [NFA+H₂O₂] were collected on a Bruker D8 Venture machine (Bruker AXS, Karlsruhe, Germany) using graphite monochromatized MoK_α radiation ($\lambda = 0.71073 \text{ \AA}$) at 100 and 150 K, respectively. The absorption corrections based on measurements of equivalent reflections were applied [56]. The structures were solved by direct methods and refined by full matrix least-squares on F^2 with anisotropic thermal parameters for all non-hydrogen atoms [57]. All hydrogen atoms were found from difference Fourier synthesis and refined isotropically. The experimental details are listed in Table 2.

The crystallographic data for [2AmNic+Mle+H₂O₂] and [NFA+H₂O₂] were deposited with the Cambridge Crystallographic Data Centre as supplementary publications under the CCDC numbers 2115827 and 2115828, respectively.

3.4. Raman Spectroscopy

The Raman measurements in the spectral range of 10–2000 cm^{−1} were conducted using a Raman microscope (inVia, Renishaw plc, Spectroscopy Product Division, Old Town Wotton-Under-Edge, Gloucestershire, UK) with the 50× objective lens (Leica DM 2500 M, NA = 0.75, Leica Mikrosysteme Vertrieb gmbH Mikroskopie und HistologieErnst-Leitz-Strasse 17-37, Wetzlar, Germany). The measurements in the spectral range of 10–200 cm^{−1} were made with a NExT monochromator, whereas in the spectral range 200–2000 cm^{−1} they were made with an edge-filter. The excitation wavelength was 633 nm, being provided by a He-Ne laser (RL633, Renishaw) with the maximum power of 17 mW. The acquisition time and number of accumulations were adjusted to maximize the signal-to-noise ratio with the minimal sample degradation. All the spectra for the powder samples were measured at several points and then averaged to reduce the anisotropy effect on the Raman spectra and to increase the single-to-noise ratio. The background from the Raman spectra was subtracted by the cubic spline interpolation method. All the spectra were divided by the number of accumulations and acquisition time.

3.5. Periodic (Solid-State) DFT Computations

The Kohn–Sham methods with periodic boundary conditions (periodic DFT) provide a grounded trade-off between the accuracy and the rate of calculations of experimentally observed properties of multi-component organic crystals [58–60]. The computations with all-electron Gaussian-type localized orbital basis 6-31G** were conducted using the CRYSTAL17 package [61]. B3LYP [62,63] and PBE [64] were employed. The London dispersion interactions were taken into account by introducing the D3 correction with Becke-Jones damping (PBE-D3) developed by Grimme et al. [65]. The space groups and the unit cell parameters of the crystals obtained from the X-ray diffraction experiment were fixed and the structural relaxations were limited to the positional parameters of the atoms (AtomOnly). Further details of the periodic DFT calculations are given in the Supporting Information.

4. Conclusions

According to the structural databases, there are 103 peroxosolvates, 91 of which are organic crystals. After excluding crystals with structurally disordered H₂O₂ molecules, crystals in which H₂O₂ molecules directly interact with the Li⁺, Na⁺, K⁺, NH₄⁺ ions or with other H₂O₂ molecules, the number of analyzed peroxosolvates decreased to 38. In these crystals, H₂O₂ interacts with the surrounding organic molecules through H-bonds. We concluded the following: (i) H₂O₂ does not form classical H-bonds as a proton acceptor if the organic cofomers do not have active hydrogen atoms. Such crystals make up a significant proportion of the considered crystals (43%). (ii) H₂O₂ forms three or four H-bonds as a proton acceptor in five crystals. The oxygen atoms of H₂O₂ are less likely to participate in bifurcate H-bonds than the C=O and P=O groups. (iii) In the remaining 46% of crystals, the H₂O₂ molecule forms one or two bonds as a proton acceptor. (iv) Currently, there are only a few examples of a bifurcate H-bond formed by the OH group of H₂O₂.

These findings allow suggesting that suitable H-bond acceptors in the cofomer molecule are crucial for peroxosolvate formation, while the presence of strong H-bond donors is not mandatory.

In accord with the literature [15,16], the enthalpies of H-bonds formed by H₂O₂ as a proton donor turned out to be higher than the values of the corresponding H-bonds formed by H₂O in the considered crystals. The enthalpy of the bifurcate H-bond formed by the OH group is significantly higher than the enthalpy of the ordinary H-bond formed by another OH group of H₂O or H₂O₂. The proton acceptor properties of H₂O are stronger than those of H₂O₂. The neutral O⋯H-O/O⋯H-N bonds formed by the lone electron pair of the oxygen atom of water turned out to be the strongest H-bonds in the considered crystals.

The bands in the low-frequency Raman spectra of the considered crystals, characterized exclusively by the vibrations of the atoms of H₂O₂ or water molecules, were not traced. Some Raman intense bands below 50 cm⁻¹ are characterized by the essential displacements of the oxygen atoms of H₂O₂ or H₂O. The displacement of the H₂O₂ molecule is negligible in the lattice vibrations [54] located in the 50–150 frequency region.

Supplementary Materials: The following are available online, Figure S1: The fragment of crystalline L-Serine hydrogen peroxide solvate (CCDC 726697) [17], Figure S2: The fragment of crystalline 5,5'-dinitro-2H,2'H-3,3'-bi-1,2,4-triazole hydrogen peroxide solvate (CCDC 1874657) [66], Table S1: Refcodes of the analyzed peroxosolvates, Figure S3: Low-frequency Raman spectrum of crystalline [NFA+H₂O]. Experiment vs. PBE-D3/6-31G** computations, Figure S4: Schematic representation of atom displacements of the two Raman intense vibrations (PBE-D3/6-31G**) of crystalline [NFA+H₂O] around 16 cm⁻¹ (a); and 64 cm⁻¹ (b). Figure S5: Low-frequency Raman spectrum of crystalline [2AmNic+Mle+H₂O]. Experiment vs. B3LYP/6-31G** computations, Figure S6: Schematic representation of atom displacements of the two Raman intense vibrations (B3LYP/6-31G**) of crystalline [2AmNic+Mle+H₂O] around 50 cm⁻¹ (a); and 72 cm⁻¹ (b), Figure S7: Raman spectrum of crystalline [NFA+H₂O₂] in the 850–950 frequency region. Experiment vs. PBE-D3 computations, Figure S8: Raman spectrum of crystalline [2AmNic+Mle+H₂O₂] in the 850–950 frequency region. Experiment vs. PBE-D3 computations, Section S1: Details of the periodic DFT calculations, Table S2: Distances between the atoms involved in the formation of intermolecular H-bonds in [2AmNic+Mle+H₂O] (1:1:1) and [2AmNic+Mle+H₂O₂] (1:1:1), $R(\text{O}\cdots\text{N})$, $R(\text{O}\cdots\text{O})$, and $R(\text{H}\cdots\text{O})$ obtained using periodic DFT computations (B3LYP/6-31G**) and the ΔH_{HB} values evaluated using Equation (1), Table S3: Distances between the atoms involved in the formation of intermolecular H-bonds in [NFA+H₂O] and [NFA+H₂O₂], $R(\text{O}\cdots\text{N})$, $R(\text{O}\cdots\text{O})$, and $R(\text{H}\cdots\text{O})$ obtained using periodic DFT computations (B3LYP/6-31G**) and the ΔH_{HB} values, evaluated using Equation (1).

Author Contributions: Conceptualization, M.V.V. and A.F.; experimental methodology, A.V.C. and A.G.M.; theoretical methodology, M.V.V.; investigation, A.V.C., A.P.V., O.D.P., S.V.A., O.A.A., D.E.M. and A.G.M.; single-crystal XRD experiment, A.V.C.; Raman spectroscopy, O.D.P.; writing and visualization, A.V.C., M.V.V. and A.F.; supervision, M.V.V. and A.F.; project administration, A.V.C.; funding acquisition, A.F. All authors have read and agreed to the published version of the manuscript.

Funding: The synthesis of peroxosolvates and X-ray structural analysis of their crystal structure were carried out with the financial support of the Russian Foundation for Basic Research (project No 20-03-00449, 18-29-19119). Periodic DFT calculations presented in this work were carried out with the financial support of the Russian Science Foundation (project No 19-73-10005).

Institutional Review Board Statement: Not applicable.

Informed Consent Statement: Not applicable.

Data Availability Statement: The Raman spectra and I/O files are available from the respective author upon reasonable request.

Acknowledgments: The single-crystal X-ray diffraction studies were performed at the Centre of Shared Equipment of IGIC RAS. The experimental Raman spectra were obtained at Lomonosov Moscow State University using the equipment purchased within the Lomonosov Moscow State University Program of Development. The Authors gratefully acknowledge the Wrocław Center for Networking and Supercomputing (WCSS) for generous grants of CPU time and technical support.

Conflicts of Interest: The authors declare no conflict of interest.

Sample Availability: No possibility.

References

1. Evora, A.O.L.; Castro, R.A.E.; Maria, T.M.R.; Rosado, M.T.S.; Silva, M.R.; Beja, A.M.; Canotilho, J.; Eusebio, M.E.S. Pyrazinamide-Diflunisal: A New Dual-Drug Co-Crystal. *Cryst. Growth Des.* **2011**, *11*, 4780–4788. [[CrossRef](#)]
2. Grobelny, P.; Mukherjee, A.; Desiraju, G.R. Drug-drug co-crystals: Temperature-dependent proton mobility in the molecular complex of isoniazid with 4-aminosalicylic acid. *CrystEngComm* **2011**, *13*, 4358–4364. [[CrossRef](#)]
3. Kaur, R.; Cavanagh, K.L.; Rodriguez-Hornedo, N.; Matzger, A.J. Multidrug Cocrystal of Anticonvulsants: Influence of Strong Intermolecular Interactions on Physicochemical Properties. *Cryst. Growth Des.* **2017**, *17*, 5012–5016. [[CrossRef](#)] [[PubMed](#)]
4. Sekhon, B.S. Drug-drug co-crystals. *DARU J. Pharm. Sci.* **2012**, *20*, 45. [[CrossRef](#)] [[PubMed](#)]
5. Linley, E.; Denyer, S.P.; McDonnell, G.; Simons, C.; Maillard, J.Y. Use of hydrogen peroxide as a biocide: New consideration of its mechanisms of biocidal action. *J. Antimicrob. Chemotherm.* **2012**, *67*, 1589–1596. [[CrossRef](#)] [[PubMed](#)]
6. Kersten, K.M.; Breen, M.E.; Mapp, A.K.; Matzger, A.J. Pharmaceutical solvate formation for the incorporation of the antimicrobial agent hydrogen peroxide. *Chem. Commun.* **2018**, *54*, 9286–9289. [[CrossRef](#)] [[PubMed](#)]
7. Ahn, S.H.; Cluff, K.J.; Bhuvanesh, N.; Blümel, J. Hydrogen Peroxide and Di(hydroperoxy)propane Adducts of Phosphine Oxides as Stoichiometric and Soluble Oxidizing Agents. *Angew. Chem. Int. Ed.* **2015**, *54*, 13341–13345. [[CrossRef](#)] [[PubMed](#)]
8. Hilliard, C.R.; Bhuvanesh, N.; Gladysz, J.A.; Blümel, J. Synthesis, purification, and characterization of phosphine oxides and their hydrogen peroxide adducts. *Dalton Trans.* **2012**, *41*, 1742–1754. [[CrossRef](#)] [[PubMed](#)]
9. Churakov, A.V.; Grishanov, D.A.; Medvedev, A.G.; Mikhaylov, A.A.; Vener, M.V.; Navasardyan, M.A.; Tripol'skaya, T.A.; Lev, O.; Prikhodchenko, P.V. Stabilization of hydrogen peroxide by hydrogen bonding in the crystal structure of 2-aminobenzimidazole perhydrate. *Cryst. Eng. Comm.* **2020**, *22*, 2866–2872. [[CrossRef](#)]
10. Foroughi, L.M.; Metzger, A.J. From Hydrate to Peroxosolvate: A Test of Prediction with Cyclic N-Oxides. *Cryst. Growth Des.* **2021**, *21*, 5873–5879. [[CrossRef](#)]
11. Luo, J.; Xia, H.; Zhang, W.; Song, S.; Zhang, Q. A promising hydrogen peroxide adduct of ammonium cyclopentazolate as a green propellant component. *J. Mater. Chem. A* **2020**, *8*, 12334–12338. [[CrossRef](#)]
12. Gillon, A.L.; Feeder, N.; Davey, R.J.; Storey, R. Hydration in Molecular Crystals—A Cambridge Structural Database Analysis. *Cryst. Growth Des.* **2003**, *3*, 663–673. [[CrossRef](#)]
13. Infantes, L.; Fabian, L.; Motherwell, W.D.S. Organic crystal hydrates: What are the important factors for formation. *CrystEngComm* **2007**, *9*, 65–71. [[CrossRef](#)]
14. Chernyshov, I.Y.; Vener, M.V.; Prikhodchenko, P.V.; Medvedev, A.G.; Lev, O.; Churakov, A.V. Peroxosolvates: Formation Criteria, H₂O₂ Hydrogen Bonding, and Isomorphism with the Corresponding Hydrates. *Cryst. Growth Des.* **2017**, *17*, 214–220. [[CrossRef](#)]
15. Vener, M.V.; Medvedev, A.G.; Churakov, A.V.; Prikhodchenko, P.V.; Tripol'skaya, T.A.; Lev, O. H-Bond Network in Amino Acid Cocrystals with H₂O or H₂O₂. The DFT Study of Serine–H₂O and Serine–H₂O₂. *J. Phys. Chem. A* **2011**, *115*, 13657–13663. [[CrossRef](#)] [[PubMed](#)]
16. Medvedev, A.G.; Shishkina, A.V.; Prikhodchenko, P.V.; Lev, O.; Vener, M.V. The Applicability of the Dimeric Heterosynthon Concept to Molecules with Equivalent Binding Sites. A DFT Study of Crystalline Urea–H₂O₂. *RSC Adv.* **2015**, *5*, 29601–29608. [[CrossRef](#)]
17. Churakov, A.V.; Prikhodchenko, P.V.; Howard, J.A.K.; Lev, O. Glycine and L-serine Crystalline Perhydrates. *Chem. Commun.* **2009**, 4224–4226. [[CrossRef](#)]
18. Prikhodchenko, P.V.; Medvedev, A.G.; Tripol'skaya, T.A.; Churakov, A.V.; Wolanov, Y.; Howard, J.A.K.; Lev, O. Crystal Structures of Natural Amino Acid Perhydrates. *CrystEngComm* **2011**, *13*, 2399–2407. [[CrossRef](#)]
19. Yamaguchi, R.; Tanaka, R.; Maetani, M.; Tabe, H.; Yamada, Y. Efficient capturing of hydrogen peroxide in dilute aqueous solution by co-crystallization with amino acids. *CrystEngComm* **2021**, *23*, 5456–5462. [[CrossRef](#)]
20. Steiner, T. The Hydrogen Bond in the Solid State. *Angew. Chem. Int. Ed.* **2002**, *41*, 48–76. [[CrossRef](#)]
21. Herschlag, D.; Pinney, M.M. Hydrogen Bonds: Simple after All? *Biochemistry* **2018**, *57*, 3338–3352. [[CrossRef](#)] [[PubMed](#)]
22. Musin, R.N.; Mariam, Y.H. An integrated approach to the study of intramolecular hydrogen bonds in malonaldehyde enol derivatives and naphthazarin: Trend in energetic versus geometrical consequences. *J. Phys. Org. Chem.* **2006**, *19*, 425–444. [[CrossRef](#)]
23. Vener, M.V.; Levina, E.O.; Astakhov, A.A.; Tsirelson, V.G. Specific Features of the Extra Strong Intermolecular Hydrogen Bonds in Crystals: Insights from the Theoretical Charge Density Analysis. *Chem. Phys. Lett.* **2015**, *638*, 233–236. [[CrossRef](#)]
24. Iogansen, A.V. Direct Proportionality of the Hydrogen Bonding Energy and the Intensification of the Stretching XH Vibration in Infrared Spectra. *Spectrochim. Acta A* **1999**, *55*, 1585–1612. [[CrossRef](#)]
25. Rozenberg, M.; Loewenschuss, A.; Marcus, Y. An Empirical Correlation Between Stretching Vibration Redshift and Hydrogen Bond Length. *Phys. Chem. Chem. Phys.* **2000**, *2*, 2699–2702. [[CrossRef](#)]
26. Rozenberg, M.; Shoham, G.; Reva, I.; Fausto, R. A correlation between the proton stretching vibration red shift and the hydrogen bond length in polycrystalline amino acids and peptides. *Phys. Chem. Chem. Phys.* **2005**, *7*, 2376–2383. [[CrossRef](#)]

27. Mata, I.; Alkorta, I.; Espinosa, E.; Molins, E. Relationships Between Interaction Energy, Intermolecular Distance and Electron Density Properties in Hydrogen Bonded Complexes under External Electric Fields. *Chem. Phys. Lett.* **2011**, *507*, 185–189. [[CrossRef](#)]
28. Medvedev, A.G.; Churakov, A.V.; Prikhodchenko, P.V.; Lev, O.; Vener, M.V. Crystalline Peroxosolvates: Nature of the Cofomer, Hydrogen-Bonded Networks and Clusters, Intermolecular Interactions. *Molecules* **2021**, *26*, 26. [[CrossRef](#)]
29. Yukhnevich, G.V. Relationship Between the Lengths of Covalent and Intermolecular Bonds in X-HY bridges. *Crystallogr. Rep.* **2010**, *55*, 377–380. [[CrossRef](#)]
30. Evarestov, R.A. *Quantum Chemistry of Solids*; Springer: Berlin/Heidelberg, Germany, 2012; pp. 1–734. [[CrossRef](#)]
31. Deringer, V.L.; George, J.; Dronskowski, R.; Englert, U. Plane-Wave Density Functional Theory Meets Molecular Crystals: Thermal Ellipsoids and Intermolecular Interactions. *Acc. Chem. Res.* **2017**, *50*, 1231–1239. [[CrossRef](#)]
32. Churakov, A.V.; Grishanov, D.A.; Medvedev, A.G.; Mikhaylov, A.A.; Tripol'skaya, T.A.; Vener, M.V.; Navasardyan, M.A.; Lev, O.; Prikhodchenko, P.V. Cyclic Dipeptide Peroxosolvates: First Direct Evidence for Hydrogen Bonding Between Hydrogen Peroxide and a Peptide Backbone. *CrystEngComm* **2019**, *21*, 4961–4968. [[CrossRef](#)]
33. Groom, C.R.; Bruno, I.J.; Lightfoot, M.P.; Ward, S.C. The Cambridge Structural Database. *Acta Cryst.* **2016**, *B72*, 171–179. [[CrossRef](#)]
34. Belsky, A.; Hellenbrandt, M.; Karen, V.L.; Luksch, P. New developments in the Inorganic Crystal Structure Database (ICSD): Accessibility in support of materials research and design. *Acta Cryst.* **2002**, *B58*, 364–369. [[CrossRef](#)]
35. Pienaar, E.W.; Caira, M.R.; Lotter, A.P. Polymorphs of nitrofurantoin. I. Preparation and X-ray crystal structures of two monohydrated forms of nitrofurantoin. *J. Crystallogr. Spectrosc. Res.* **1993**, *23*, 739–744. [[CrossRef](#)]
36. Surov, A.O.; Vasilev, N.A.; Churakov, A.V.; Parashchuk, O.D.; Artobolevskii, S.V.; Alatorsev, O.A.; Makhrov, D.E.; Vener, M.V. Two Faces of Water in the Formation and Stabilization of Multicomponent Crystals of Zwitterionic Drug-Like Compounds. *Symmetry* **2021**, *13*, 425. [[CrossRef](#)]
37. Tupikina, E.Y.; Bodensteiner, M.; Tolstoy, P.M.; Denisov, G.S.; Shenderovich, I.G. P=O Moiety as an Ambidextrous Hydrogen Bond Acceptor. *J. Phys. Chem. C* **2018**, *122*, 1711–1720. [[CrossRef](#)]
38. Bennion, J.C.; Chowdhury, N.; Kampf, J.W.; Matzger, A.J. Hydrogen Peroxide Solvates of 2,4,6,8,10,12-Hexanitro-2,4,6,8,10,12-hexaazaisowurtzitane. *Angew. Chem. Int. Ed.* **2016**, *55*, 13118–13121. [[CrossRef](#)]
39. Manin, A.N.; Voronin, A.P.; Shishkina, A.V.; Vener, M.V.; Churakov, A.V.; Perlovich, G.L. Influence of Secondary Interactions on the Structure, Sublimation Thermodynamics, and Solubility of Salicylate:4-Hydroxybenzamide Cocrystals. Combined Experimental and Theoretical Study. *J. Phys. Chem. B* **2015**, *119*, 10466–10477. [[CrossRef](#)] [[PubMed](#)]
40. Taylor, R. It Isn't, It Is: The C–H...X (X = O, N, F, Cl) Interaction Really Is Significant in Crystal Packing. *Cryst. Growth Des.* **2016**, *16*, 4165–4168. [[CrossRef](#)]
41. Tuma, C.; Boese, D.A.; Handy, N.C. Predicting the binding energies of H-bonded complexes: A comparative DFT study. *Phys. Chem. Chem. Phys.* **1999**, *1*, 3939–3947. [[CrossRef](#)]
42. Vener, M.V.; Levina, E.O.; Koloskov, O.A.; Rykounov, A.A.; Voronin, A.P.; Tsirelson, V.G. Evaluation of the lattice energy of the two-component molecular crystals using solid-state density functional theory. *Cryst. Growth Des.* **2014**, *14*, 4997–5003. [[CrossRef](#)]
43. Medvedev, A.G.; Mikhaylov, A.A.; Chernyshov, I.Y.; Vener, M.V.; Lev, O.; Prikhodchenko, P.V. Effect of aluminum vacancies on the H₂O₂ or H₂O interaction with a gamma-AlOOH surface. A solid-state DFT study. *Int. J. Quantum Chem.* **2019**, *119*, e25920. [[CrossRef](#)]
44. Parrott, E.P.J.; Zeitler, J.A. Terahertz Time-Domain and Low-Frequency Raman Spectroscopy of Organic Materials. *Appl. Spectrosc.* **2015**, *69*, 1–25. [[CrossRef](#)] [[PubMed](#)]
45. King, M.D.; Buchanan, W.D.; Korter, T.M. Identification and Quantification of Polymorphism in the Pharmaceutical Compound Diclofenac Acid by Terahertz Spectroscopy and Solid-State Density Functional Theory. *Anal. Chem.* **2011**, *83*, 3786–3792. [[CrossRef](#)]
46. Zhang, F.; Wang, H.-W.; Tominaga, K.; Hayashi, M. Mixing of intermolecular and intramolecular vibrations in optical phonon modes: Terahertz spectroscopy and solid-state density functional theory. *WIREs Comput. Mol. Sci.* **2016**, *6*, 386–409. [[CrossRef](#)]
47. Vener, M.V.; Parashchuk, O.D.; Kharlanov, O.G.; Maslennikov, D.R.; Dominskiy, D.I.; Chernyshov, I.Y.; Parashchuk, D.Y.; Sosorev, A.Y. Non-Local Electron-Phonon Interaction in Naphthalene Diimide Derivatives, its Experimental Probe and Impact on Charge-Carrier Mobility. *Adv. Electron. Mater.* **2021**, *7*, 2001281. [[CrossRef](#)]
48. Takahashi, M. Terahertz Vibrations and Hydrogen-Bonded Networks in Crystals. *Crystals* **2014**, *4*, 74–103. [[CrossRef](#)]
49. Surov, A.O.; Vasilev, N.A.; Vener, M.V.; Parashchuk, O.D.; Churakov, A.V.; Magdysyuk, O.V.; Perlovich, G.L. Pharmaceutical Salts of Fenbendazole with Organic Counterions: Structural Analysis and Solubility Performance. *Cryst. Growth Des.* **2021**, *21*, 4516–4530. [[CrossRef](#)]
50. Vener, M.V.; Chernyshov, I.Y.; Rykounov, A.A.; Filarowski, A. Structural and Spectroscopic Features of Proton Hydrates in the Crystalline State. Solid-state DFT Study on HCl and Triflic Acid Hydrates. *Mol. Phys.* **2018**, *116*, 251–262. [[CrossRef](#)]
51. Scott, A.P.; Radom, L.J. Harmonic Vibrational Frequencies: An Evaluation of Hartree–Fock, Møller–Plesset, Quadratic Configuration Interaction, Density Functional Theory, and Semiempirical Scale Factors. *J. Phys. Chem.* **1996**, *100*, 16502–16513. [[CrossRef](#)]
52. Sosorev, A.Y.; Maslennikov, D.; Chernyshov, I.Y.; Dominskiy, D.I.; Bruevich, V.V.; Vener, M.V.; Parashchuk, D.Y. Relationship between electron–phonon interaction and low-frequency Raman anisotropy in high-mobility organic semiconductors. *Phys. Chem. Chem. Phys.* **2018**, *20*, 18912–18918. [[CrossRef](#)] [[PubMed](#)]

53. Grishanov, D.A.; Navasardyan, M.A.; Medvedev, A.G.; Lev, O.; Prikhodchenko, P.V.; Churakov, A.V. Hydrogen Peroxide Insular Dodecameric and Pentameric Clusters in Peroxosolvate Structures. *Angew. Chem. Int. Ed.* **2017**, *56*, 15241–15245. [[CrossRef](#)] [[PubMed](#)]
54. Bi, J.; Tao, Y.; Hu, J.-Y.; Wang, H.; Zhou, M. High-pressure investigations on urea hydrogen peroxide. *Chem. Phys. Lett.* **2022**, *787*, 139230. [[CrossRef](#)]
55. Giguere, P.A.; Geoffrion, P. Refractive index of hydrogen peroxide solutions. A revision. *Can. J. Res.* **1949**, *27B*, 168–173. [[CrossRef](#)]
56. Sheldrick, G.M. *SADABS, Program for Scaling and Correction of Area Detector Data*; University of Göttingen: Göttingen, Germany, 1997.
57. Sheldrick, G.M. Crystal structure refinement with SHELXL. *Acta. Crystallogr.* **2015**, *C71*, 3–8.
58. Fonari, A.; Corbin, N.S.; Vermeulen, D.; Goetz, K.P.; Jurchescu, O.D.; McNeil, L.E.; Bredas, J.L.; Coropceanu, V. Vibrational properties of organic donor-acceptor molecular crystals: Anthracene-pyromellitic-dianhydride (PMDA) as a case study. *J. Chem. Phys.* **2015**, *143*, 224503. [[CrossRef](#)]
59. Mazurek, A.H.; Szeleszczuk, Ł.; Pisklak, D.M. Periodic DFT Calculations—Review of Applications in the Pharmaceutical Sciences. *Pharmaceutics* **2020**, *12*, 415. [[CrossRef](#)] [[PubMed](#)]
60. Voronin, A.P.; Surov, A.O.; Churakov, A.V.; Parashchuk, O.D.; Rykounov, A.A.; Vener, M.V. Combined X-ray Crystallographic, IR/Raman Spectroscopic, and Periodic DFT Investigations of New Multicomponent Crystalline Forms of Anthelmintic Drugs: A Case Study of Carbendazim Maleate. *Molecules* **2020**, *25*, 2386. [[CrossRef](#)] [[PubMed](#)]
61. Dovesi, R.; Erba, A.; Orlando, R.; Zicovich-Wilson, C.M.; Civalieri, B.; Maschio, L.; Rérat, M.; Casassa, S.; Baima, J.; Salustro, S.; et al. Quantum-mechanical condensed matter simulations with CRYSTAL. *WIREs Comput. Mol. Sci.* **2018**, *8*, e1360. [[CrossRef](#)]
62. Becke, A.D. Density-functional thermochemistry. III. The role of exact exchange. *J. Chem. Phys.* **1993**, *98*, 5648–5652. [[CrossRef](#)]
63. Vosko, S.H.; Wilk, L.; Nusair, M. Accurate spin-dependent electron liquid correlation energies for local spin density calculations: A critical analysis. *Can. J. Phys.* **1980**, *58*, 1200–1211. [[CrossRef](#)]
64. Perdew, J.P.; Burke, K.; Ernzerhof, M. Generalized Gradient Approximation Made Simple. *Phys. Rev. Lett.* **1996**, *77*, 3865–3868. [[CrossRef](#)] [[PubMed](#)]
65. Grimme, S.; Ehrlich, S.; Goerigk, L. Effect of the damping function in dispersion corrected density functional theory. *J. Comput. Chem.* **2011**, *32*, 1456–1465. [[CrossRef](#)] [[PubMed](#)]
66. Wiscons, R.A.; Bellas, M.K.; Bennion, J.C.; Matzger, A.J. Detonation Performance of Ten Forms of 5,5'-Dinitro-2H,2H'-3,3'-bi-1,2,4-triazole (DNBT). *Cryst. Growth Des.* **2018**, *18*, 7701–7707. [[CrossRef](#)]